

1 **Model Test Research of a Semisubmersible Floating Wind**
2 **Turbine with an Improved Deficient Thrust Force**
3 **Correction Approach**

4 Liang Li^{a,c}, Yan Gao^{a,*}, Zhiqiang Hu^{b,c}, Zhiming Yuan^a, Sandy Day^a, Haoran Li^c

5 ^a*Department of Naval Architecture Ocean and Marine Engineering, University of Strathclyde, 100*
6 *Montrose Street, Glasgow G4 0LZ, United Kingdom*

7 ^b*School of Marine Science and Technology, Newcastle University, Newcastle upon Tyne*
8 *NE1 7RU, United Kingdom*

9 ^c*State Key Laboratory of Ocean Engineering, Shanghai Jiao Tong University, Shanghai 800 Donchuan*
10 *Road, 200240, China*

11 *Corresponding author: Department of Naval Architecture Ocean and Marine Engineering, University*
12 *of Strathclyde, 100 Montrose Street, Glasgow G4 0LZ, United Kingdom*

13 *E-mail address: yan.gao@strath.ac.uk*

14 **ABSTRACT**

15 This paper investigates the model test research of a semisubmersible floating wind turbine.
16 An improved method is proposed to correct the deficient thrust force in a Froude-scale
17 experimental condition, which is able to simulate the rotor operational state more realistically
18 by allowing the rotor to rotate freely with the wind. This approach also maintains tip speed
19 ratio to some extent and overcomes previously reported negative effects produced by common
20 correction ways. Reduced platform resonant motions in the presence of wind force are
21 observed. Due to rotor rotation, resonant yaw and roll motions are induced even in heading
22 wind and wave state. Tower vibration is found to be suppressed by the wind force.
23 Multi-frequencies components are observed in the response of tower-top shear force, which is
24 governed by the couplings of hydrodynamic loads, aerodynamic loads and tower vibration. It
25 is also found that the dynamic response of the mooring line is mainly dominated by wave load
26 and aerodynamic effect can be simplified as an extra constant force.

27 *Key words:* floating wind turbine; model test; thrust force correction approach, renewable
28 energy, hydrodynamic load, aerodynamic load;

1. Introduction

Due to issues like environmental pollution, energy crisis and sustainable development, the development of wind energy industry has been boosted by the global pursuit of renewable energy. Although the commercial application of onshore wind turbines has been proved successful, the traditional land-based wind turbines are continually complained about the visual, acoustic and environmental impacts. Besides, it is technologically difficult to achieve high energy efficiency from onshore wind resource as a result of turbulent wind farm and low annual mean wind velocity. Therefore, the wind energy industry is trying to exploit the high-quality wind resource in deep water zones.

A series of floating wind turbine concepts have been proposed all over the world. Statoil launched a spar-buoy floating wind turbine project, namely the Hywind concept [1], which is the first full scale floating wind turbine that has ever been built. Roddier et al. [2] made efforts on the feasibility study of the WindFloat concept, a three-column submersible floating foundation for offshore wind turbine [3-5]. Karimirad and Michailides [6] proposed a V-shaped semisubmersible offshore wind turbine. Li et al. [7] studied the dynamic response of a spar type floating wind turbine when incorporated with a wave energy converter and two tidal turbines.

The study of floating wind turbine is multi-disciplinary, involving hydrodynamics, aerodynamics, control algorithm, modeling of structure and multi-body dynamics. Borg and Collu [8] discussed the approach of developing a coupled numerical model for floating wind turbine, considering aerodynamics, hydrodynamics, structural deflection, mooring line dynamics and control scheme. Martin [9] presented detailed information on scaling methodology, design and physical characterization of the NREL's baseline wind turbine for the application in model test. Farrugia et al. [10] studied wave motions effects on wind turbine rotor aerodynamics using lifting line method. Salehyar and Zhu [11] examined the aerodynamic dissipation effect on the wind turbine blades with a quasi-static approach and an unsteady approach, respectively. Larsen and Hanson [12] presented an improved control algorithm to overcome the negative damping caused by blade pitch control for over rated

57 wind velocities. Odgaard et al. [13] used Pareto curves to tune a linear model predictive
58 controller for wind turbines.

59 Based on the development of basic principles, simulation tools are proposed for the fully
60 coupled analysis of floating wind turbines. Jonkman [14] developed a hydrodynamic module
61 and implemented it to FAST. Skaare et al. [15] came up with a new computational tool on the
62 basis of aerodynamic code HAWC2 and hydrodynamic, structural and control system analysis
63 tools SIMO/RIFLEX. Li et al. [16] developed a aero-hydro dynamic code for analysis of
64 floating wind turbine. Quallen and Xing [17] developed a simulation tool with a
65 variable-speed generator-torque controller using CFD calculation method.

66 Although a series of simulation tools have been developed, the validations of these tools
67 still rely on comparative code-to-code check analysis due to the lack of reliable model test
68 results. The validation work based on model test method has not been adequately conducted.
69 With the collaboration of a group of research institutes, including NREL, MAINE University
70 and MARIN etc., projects OC3 and OC4 started the steps of validating numerical tools and
71 also obtaining floating wind turbine's dynamic characters through the technique of basin
72 model test [18, 19]. Duan et al. [20] investigates the dynamic response of a spar-buoy floating
73 wind turbine with model test approach. Nevertheless, few test data are open to the public and
74 researchers usually find it difficult to validate their in-house numerical codes.

75 Model test technique provides not only a reliable source to validate numerical analysis
76 codes, but also a good approach to demonstrate the dynamic characters of the floating system,
77 especially those unable to be captured by numerical simulations. For the purpose of fully
78 studying the dynamic response of floating wind turbine and also providing model test results
79 for the validation of numerical codes, a model test research for a 5MW wind turbine is
80 conducted in Shanghai Jiao Tong University. Firstly, the set-up of the model test is presented.
81 Identification test results are given subsequently to calibrate the floating wind turbine model
82 and the environmental conditions. Afterwards, the experimental data for various test cases are
83 presented to demonstrate the dynamic characters of the floating wind turbine. Finally,
84 conclusions drawn from the model test research are presented.

2. Model test set-up

To fully understand the response mechanism of floating wind turbine under hydrodynamic and aerodynamic excitations, a large-scale model test program is launched in the Deepwater Offshore Basin at Shanghai Jiao Tong University. The water basin, equipped with advanced wave-generating system, current-generating system, wind-generating system and other testing facilities, is 50m in length, 40m in width and 10m in depth. The model test is conducted at a Froude scale of 1:50. The water depth is set as 4m corresponding to the full-scale depth of 200m. As shown in Fig. 1, the OC4-DeepCwind concept [21] is used in the test. Nevertheless, some modifications for the floating foundation and the mooring system are made due to the restrictions caused by turbine model manufacturing and installation of data measurement devices.

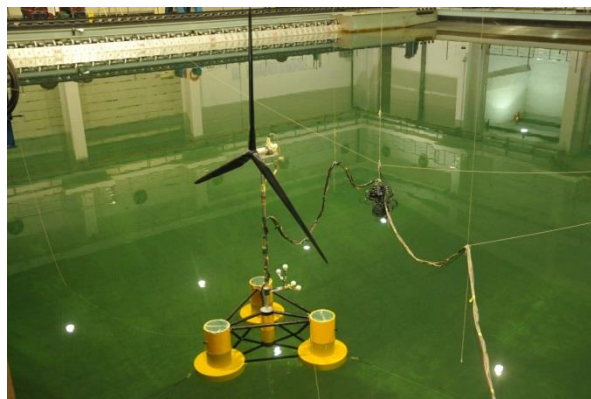


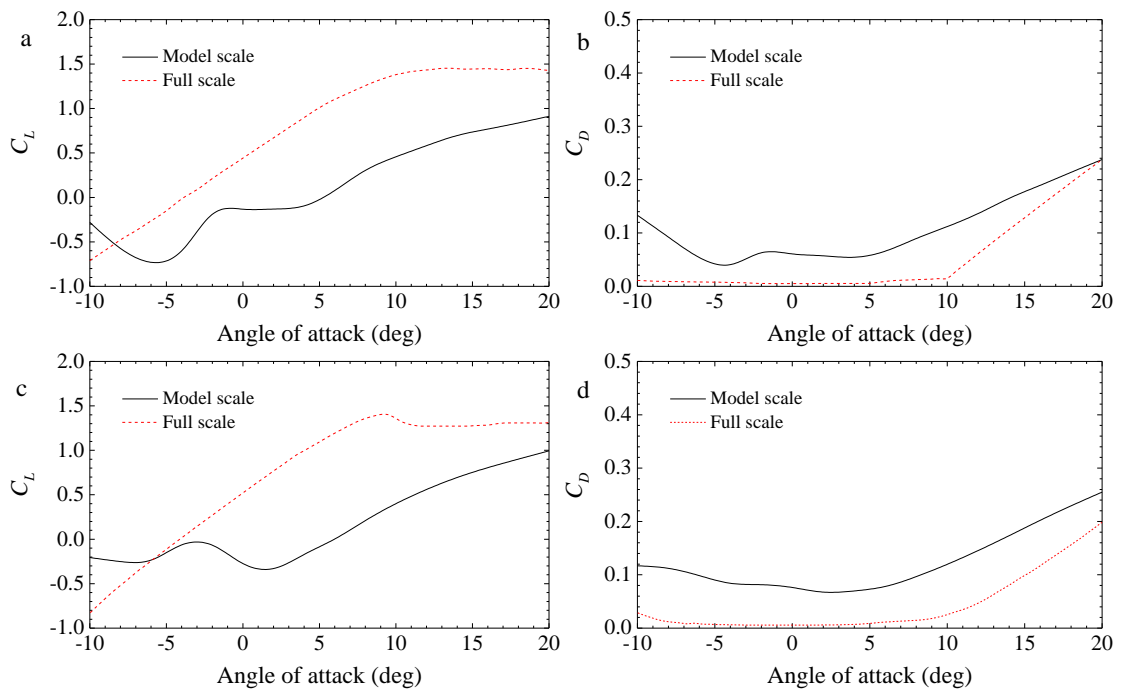
Fig. 1. Model of semisubmersible floating wind turbine

2.1 Scaling methodology and deficient thrust force correction approach

Both hydrodynamics and aerodynamics should be regarded as dominating factors in the model test research of a floating wind turbine. Froude number similitude is typically employed in water basin test to ensure the relationship between inertial and gravitational wave forces. Meanwhile, Reynolds number similarity is more common in wind tunnel test as it preserves the relationship between viscous and inertial forces of incident flow. It is ideal to maintain Froude number and Reynolds number similitude simultaneously in the test. From a practical perspective of view, however, it is impossible to achieve such a goal. Therefore, a

106 priority of the two scaling schemes should be selected. In a water basin test, a Froude-scaled
 107 model is able to cover most of the crucial properties which govern the dynamic responses of a
 108 floating body in waves. It is straightforward to employ the hydrodynamic view and maintain
 109 the Froude number in the test program. Therefore, both the floating wind turbine model and
 110 the incident waves are scaled with Froude number similitude in the model test.

111 As Froude scale method is applied in the model test, the Reynolds number similitude is
 112 no longer satisfied and the aerodynamic performance of the wind turbine will change. To
 113 demonstrate Reynolds number effect, XFOIL [22] is used to calculate the lift coefficient C_L
 114 and drag coefficient C_D of the blade airfoil at full scale ($Re = 1.15 \times 10^7$) and model scale ($Re = 3.25 \times 10^4$),
 115 respectively (see Fig. 2). The results show that C_L is reduced whereas C_D is
 116 increased at the model scale compared with prototype design. The thrust force coefficient C_T
 117 is subsequently computed with FAST [23] and the results are displayed in Fig. 3. Apparently,
 118 the model scale thrust force is much lower than the prototype value if no correction approach
 119 is applied.



120
 121 Fig. 2. Aerodynamic performance of blade airfoil at full scale and model scale. (a) C_L , NACA64_A17;
 122 (b) C_D , NACA64_A17; (c) C_L , DU21_A17; (d) C_D , DU21_A17.

123

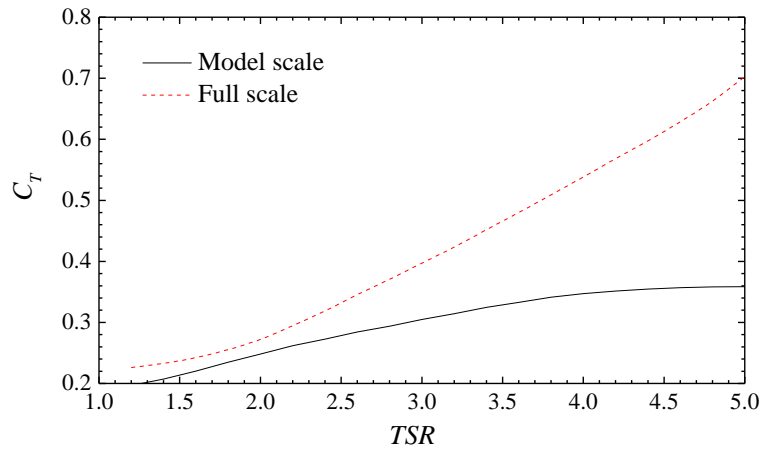


Fig. 3. Variation of thrust force coefficient with respect to tip speed ratio (TSR), blade pitch angle is fixed at 0 deg.

Most correction methods are based on increasing the model scale wind speed while utilizing an electric motor to drive the rotor. In this way, rotor speed can be exactly tuned and the designed thrust force is obtained by increasing wind speed massively. However, the TSR is no longer maintained, which ensures that the system excitation resulting from rotor imbalance or aerodynamic interaction with the tower will possess the correct frequency [24]. This type of correction method may also lead to undesirable force on the tower and the platform hull above water surface since the wind speed is significantly increased [9]. Besides, the generator is not simulated properly as it drives the rotor rather than being driven by the rotor. In the test program, we introduce an improved approach to acquire the designed thrust force and better simulate the generator operation state. Instead of being driven by an electric motor, the rotor is purely driven by the wind. The electric motor is merely used to represent the wind turbine generator. By adjusting the wind speed gradually, the thrust force acting on the rotor is recorded. The adjusting of rotor speed is achieved by an appropriate selection of the motor among several available motors with different resistance properties. In this way, the TSR can be tuned although not exactly. After a series of tests, the most favorable motor is selected and the measured relationships between thrust force, wind speed, rotor speed and TSR are outlined in Table 1. It should be noted that the relationships in Table 1 will differ when a different motor is used.

146 **Table 1**
 147 Relationship between thrust force, wind speed and rotor speed

Prototype				Measurement		
Rotor thrust (kN)	Wind speed (km/hr)	Rotor speed (rpm)	TSR	Wind speed (km/hr)	Rotor speed (rpm)	TSR
276	18	7.5	9.98	33.8	7.9	5.59
494.9	28.8	9.3	7.73	41	11.2	6.53
770.4	41	12.1	7.06	46.1	14.1	7.32
451.1	64.8	12.1	4.47	40	10.9	6.53
388.9	82.8	12.1	3.50	39	10.6	6.47
145	144	0	0	56.5	0	0

148

149 The improved correction method possesses several advantages over common ways. It is
 150 capable of simulating operation state of the rotor realistically. In model test, the relative wind
 151 speed keeps varying with platform motions and thus the rotor speed changes accordingly. It is
 152 consistent with realistic situation since the control system is active for a full scale floating
 153 wind turbine during operational condition. Besides, the shaft axial torque obtained in the
 154 model test is more reasonable compared with that acquired by common corrections ways.
 155 This is because the shaft axial torque is purely wind-driven rather than being generated by the
 156 motor. By adopting this free rotation approach, it is also able to acquire the designed thrust
 157 force without increasing the wind speed significantly. For example, the wind speed is
 158 increased from 41 km/hr to 74.9 km/hr to match the rated thrust force in the work of Martin et
 159 al. [24] while the increased wind speed is just 46 km/hr in our test. In this way, the
 160 undesirable excess drag on non-rotor structures is reduced. Furthermore, it maintains the TSR
 161 to same extent. Although the rotor speed is determined by the wind and cannot be adjusted
 162 exactly in the test, it is shown that the rotor speed changes slightly due to the appropriate
 163 selection of the motor. For example, the measured rotor speed is 14.4 rpm compared with
 164 designed value 12.1 rpm in rated thrust case.

165 *2.2 Model description*

166 *2.2.1 Wind turbine*

167 The wind turbine in the test is based on NREL's 5MW baseline wind turbine [25]. The

168 measured scantlings of turbine model are compared with prototype values in Table 2

169 **Table 2**

170 Mass and CM (center of mass) location of main components of wind turbine

Item	Prototype		Measurement	
	Mass (kg)	CM (m)	Mass (kg)	CM (m)
Blades	53,220	90	52,659	90.65
Hub	56,780	90.17	57,272	90.65
Nacelle	240,000	89.35	232,291	90.65
Tower	249,718	43.4	287,128	51
4 Identical lamps at tower bottom	-	-	27,163	30.9
1 identical lamp at tower top	-	-	6,791	92.15
Instrumentation cables	-	-	86,228	57.1
Total Wind turbine	599,718	70.35	749,532	69.45

171

172 The blades are manufactured according to geometric similitude with prototype (see Fig.
173 4). As Froude scale scheme is adopted in the test, the mass of each blade is required to be kept
174 at only 134g. From a practical perspective, it is a major challenge in the test program. Woven
175 carbon fiber material is used to meet the scaled mass target. To avoid accidental events such
176 as blades-tower collision and get rid of the aero-elastic coupling, bracing components are
177 installed inside to make the blade rigid and prevent any blade deflection. An electric motor is
178 installed at the tower-top to represent the nacelle drive-drain system and the generator. As
179 discussed above, no power is supplied to the motor and it is purely driven by wind. As no
180 control device is implemented in the test, blade-pitch angle is kept at 0° for operational cases
181 and 90° for parked cases, respectively. The shaft tilt is set 0° in the test program, instead of
182 prototype value 5° .



183
184 **Fig. 4** Blade model.

185 *2.2.2 Platform*

186 The floating foundation is made up of three main offset columns inducing buoyance and
187 restoring force, one central column supporting the wind turbine, as well as a series of diagonal
188 cross and horizontal bracing components. In order to a gain good hydrostatic stability
189 performance, a ballast tank is installed at the bottom of each main offset column. The main
190 scantlings of the platform are listed in Table 3.

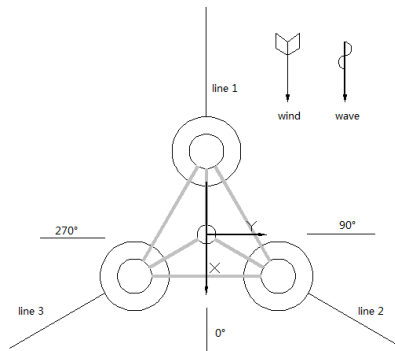
191 **Table 3**

192 Main scantlings of the platform

Term	Value
Depth of platform base below SWL	20m
Elevation of platform top above SWL	10 m
Elevation of offset columns above SWL	12 m
Spacing between offset columns	50 m
Length of upper columns	26 m
Length of base columns	6 m
Depth to top of base columns below SWL	14 m
Diameter of main column	6.5 m
Diameter of offset (upper) columns	12 m
Diameter of base columns	24 m
Platform mass	12,912,500 kg
Displacement	13,986.8 m ³
CM below CWL	13.5 m
Platform roll inertia (about CM)	6.052×10 ⁹ kg·m ²
Platform pitch inertia (about CM)	6.052×10 ⁹ kg·m ²
Platform yaw inertia (about CM)	1.201×10 ¹⁰ kg·m ²

193 *2.2.3 Mooring system design*

194 The floating wind turbine is moored at sea site with a water depth of 200m, through a
 195 mooring system composed of three taut catenary lines. Fairleads are connected to the tops of
 196 ballast tanks. Fig. 5 illustrates the coordinate system in the test. The three mooring lines are
 197 oriented symmetrically at 60°, 180°, and 300° about the vertical axis. The relevant properties
 198 of mooring lines are outlined in Table 4.



199

200 **Fig. 5.** Coordinate system and mooring system configuration

201 **Table 4**

202 Mooring system properties

Term	Value
Number of mooring lines	3
Angle between adjacent lines	120°
Depth to anchors	200 m
Depth to fairleads	14 m
Radius to anchor	853.7 m
Radius to fairleads	40.868 m
Unstretched mooring line length	835.5 m
Mooring line diameter	0.0766 m
Equivalent line mass density	113.35 kg/m
Equivalent mooring line extensional stiffness	753.6 MN

203 *2.3 Data measurement*

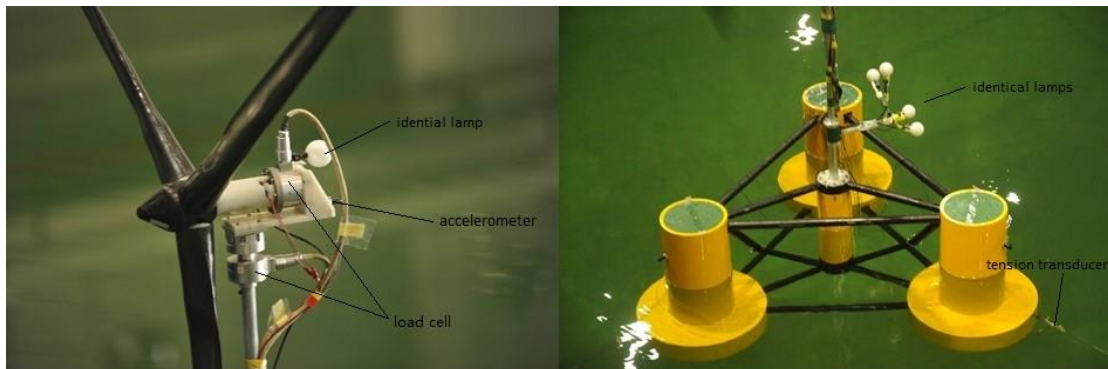
204 Advanced data acquisition techniques are used to measure the dynamic response of the
 205 floating wind turbine model. Data collection transducers are shown in Fig. 6. Motions of the
 206 nacelle and the platform are captured with a non-contact optical tracking system, which is
 207 mainly composed of positive identical lamps and capturing cameras. Tension transducers are

208 connected to the fairleads to collect mooring line tension signal. Two sets of load cells are
 209 installed. 1# load cell is installed between the nacelle and the tower structure to measure the
 210 shear force and bending moment applied at this position; and 2# load cell is installed in the
 211 rear part of the nacelle to collect the shaft axial force data. Besides, an accelerometer is also
 212 installed to measure the nacelle acceleration. Wave probes are used in the study to record time
 213 series of wave elevation. Data collection frequency is set to 20Hz for all sensors in each
 214 loading case. A summary of the data recorded in the test is listed in Table 5.

215 **Table 5**
 216 Summarization of data acquisition

Term	Location	Recorded data
Load cell	Nacelle	Shaft axial force and torque
	Tower-top	Shear force and bending moment
Accelerometer	Nacelle	Nacelle acceleration
Optical motion capture system	Nacelle	Nacelle motion
	Platform	Platform motion
Tension transducer	Fairlead	Mooring line tension force
Wave probes	Surroundings	Wave elevation

217



218

219

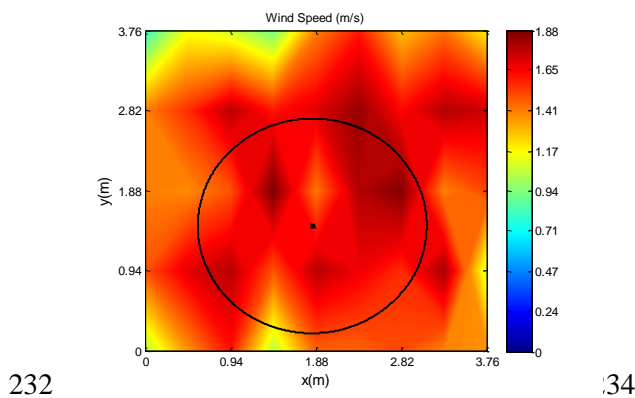
Fig. 6. Illustration of the data collection devices.

220 **3. Identification test results**

221 Prior to the basin test, a series of identification test cases are conducted. At first, the
 222 spatial homogeneity and turbulence of the generated wind field are checked. Hammer test is
 223 also performed to estimate the vibration frequency of the tower. Mooring system calibration
 224 and free decay test are followed to identify the natural periods of the floating system.

225 *3.1 Calibration of wind field*

226 Calibration test is conducted on the land to estimate the generated wind field quality. A
227 series of thermal wind speed probes are installed in front of the wind generator to form a
228 spatial matrix and measure the spatial distribution of wind speed in the virtual rotor plane,
229 which is 3 m away from the wind generator. Fig. 7 and Fig. 8 illustrate the measured wind
230 field for rated thrust force case. Detailed calibration procedures of the generated wind field
231 can be found in [26].



233 **Fig. 7.** Wind speed distribution of wind field 235

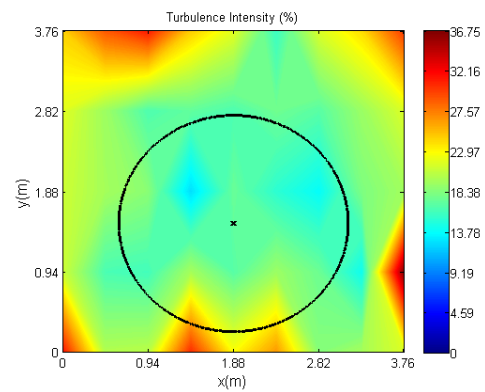
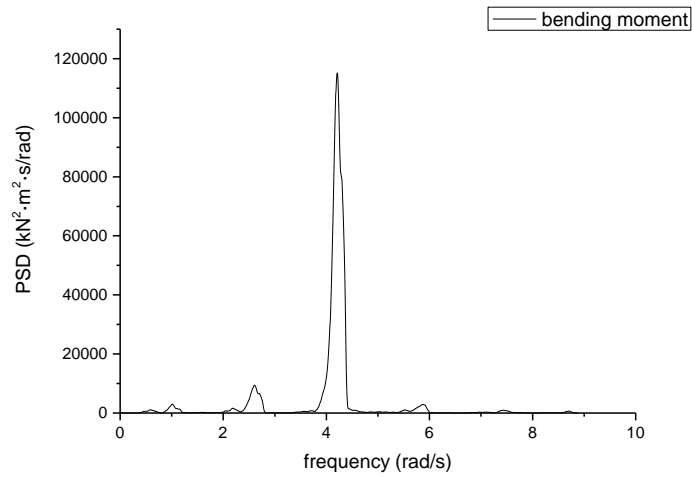


Fig. 8. Turbulence density of wind field

236 *3.2 Hammer test*

237 The vibration frequency of the tower is measured by hammer test. The tower (without
238 nacelle and rotor) is rigidly connected to the land via a load cell to record the
239 vibration-induced bending moment. An impulse excitation is afterwards applied to the
240 tower-top causing it to vibrate freely. Since the tower is axial symmetric, only fore-aft
241 impulse test is carried out. Hammer test result is illustrated in Fig. 9. The response peak is
242 observed at 2.58 rad/s and 4.21 rad/s, respectively.

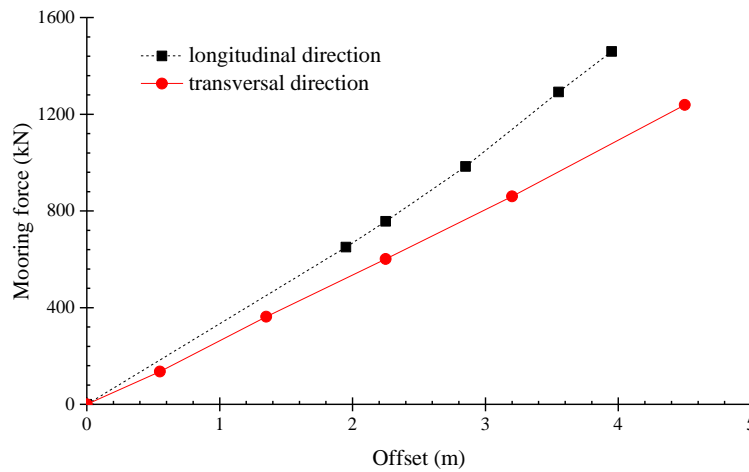


243
244

Fig. 9. Hammer test results

245 3.3 Mooring system horizontal stiffness test

246 Due to rotor rotation, the platform moves not only in longitudinal direction, but also in
247 transversal direction. Therefore, the mooring line stiffness along both longitudinal and
248 transversal directions are measured. Fig. 10 plots the measured horizontal stiffness.



249

250

Fig. 10. Measured mooring horizontal stiffness

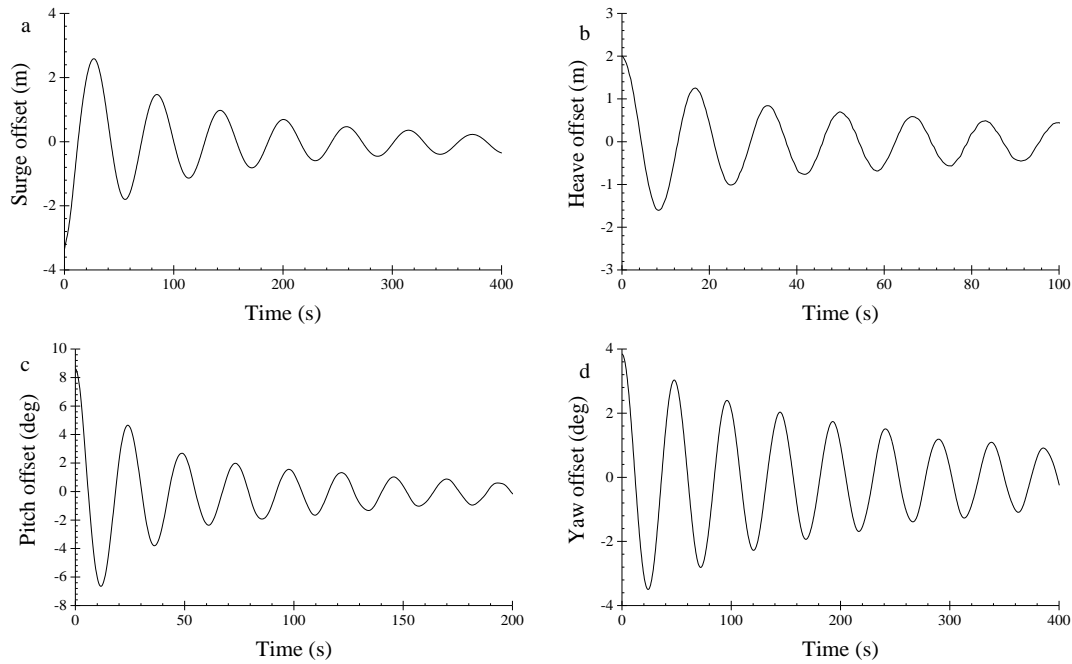
251 3.4 Free decay test

252 Natural periods of the floating system are identified with free decay test. The results of
253 free decay test are listed in Table 6. The time series of decay motions are plotted in Fig. 11.

254 **Table 6**
 255 Results of free decay tests

	Term	Surge	Heave	Pitch	Yaw
Decay test	Natural period (s)	54.546	16.390	24.492	48.225
	Damping ratio	0.0668	0.0341	0.0622	0.0285

256



257

258 **Fig. 11.** Free decay motions. (a) surge motion; (b) heave motion; (c) pitch motion; (d) yaw motion.

259

260 **4. Dynamic response of the system**

261 In the experiment program, a set of test cases are conducted to investigate platform
 262 motions, structural response and mooring line tension of the floating wind turbine. Firstly,
 263 motion response characteristics of the system are analyzed. Aerodynamic effects on platform
 264 motions and nacelle accelerations are clarified. Roll and yaw motions induced by rotor
 265 rotation are also studied. Secondly, the response mechanisms of shaft axial force and
 266 tower-top shear force are investigated. Finally, the tension force of a selected mooring line is
 267 analyzed. Table 7 presents a summary of the environmental conditions considered in the test
 268 program. The model scale duration of each test case is set 8.5 mins, corresponding to full
 269 scale 1 hour. Both wind and waves are set to propagate along the heading direction in all test

270 cases (See Fig. 5).

271 **Table 7**

272 Environmental condition definition

Case No.	Wind speed (km/hr)	Rotor speed (rpm)	Wave		
			Hs (m)	Tp (s)	γ
LC1	0	0	6	10	2.87
LC2	41	11.2	6	10	2.87
LC3	46	14.4	6	10	2.87
LC4	0	0	2	8	3.3
LC5	46	14.4	2	8	3.3

273 4.1 Platform surge and pitch motion characters

274 The platform motions under various environmental conditions are investigated. As surge
275 and pitch are critical degrees of freedom (DOF) for a floating wind turbine, this section will
276 only deal with the two DOFs. Table 8 lists the statistical results of surge and pitch motions
277 measured in test cases LC1, LC2 and LC3.

278 **Table 8**

279 Statistical results of platform surge and pitch motions

Case No.	Degree of Freedom	Max	Min	Mean	Std. dev.
LC1	Surge (m)	2.709	-1.663	0.225	0.690
	Pitch (deg)	3.330	-1.946	0.369	0.620
LC2	Surge (m)	4.652	0.301	2.137	0.651
	Pitch (deg)	5.648	1.253	3.154	0.508
LC3	Surge (m)	5.209	0.898	2.747	0.647
	Pitch (deg)	6.790	2.346	4.188	0.537

280 The statistical results show that platform motions are greatly influenced by the wind
281 force. With below-rated thrust force acting on the rotor, the mean pitch position is 3.153 deg
282 and this value increases to 4.188 deg when the system is subject to rated wind force. With
283 respect to surge motion, similar conclusion can be obtained. Mean surge position is pushed to
284 2.747 m with rated thrust force whereas it is just 0.225 m in LC1. Furthermore, it points out
285 that the standard deviations of surge and pitch motions are both somewhat reduced by the
286 wind force. To further investigate platform motions under wave & wind excitations, the
287 time-series of platform motions are analyzed with fast Fourier transform (FFT) method to
288 obtain the power spectrum density (see Fig. 12).

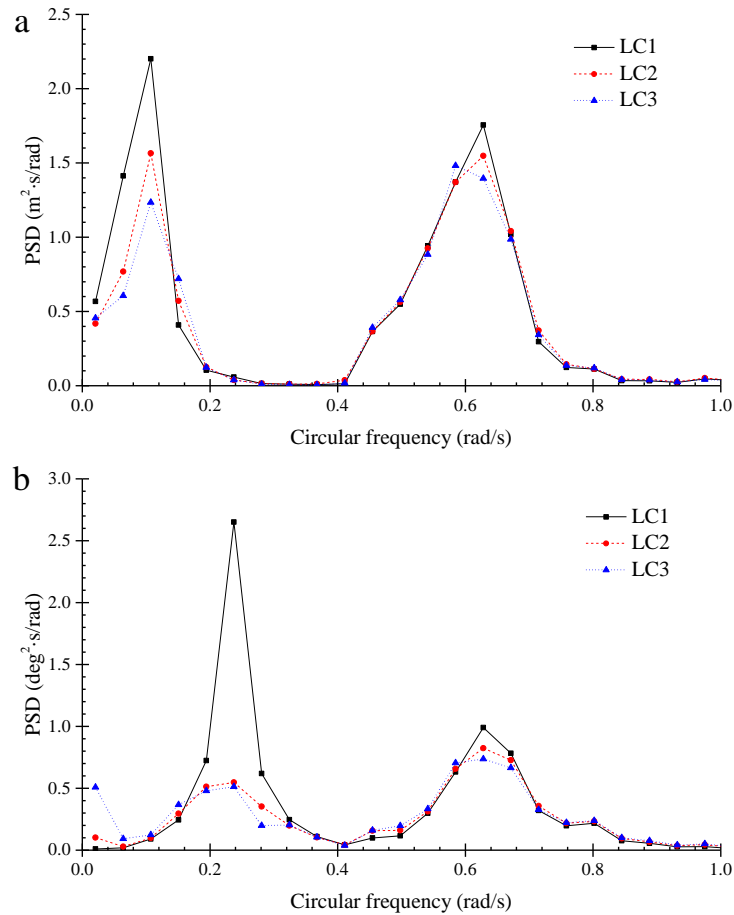


Fig. 12. Power spectrum density of platform motions. (a) surge motion; (b) pitch motion.

289

290

291

292

293

294

295

296

297

298

299

300

With consideration of the wind force, the resonant motions of surge and pitch are reduced significantly while little change is observed around the wave energy frequency range. Motions are observed within range from 0.4 rad/s to 0.9 rad/s , which are mainly wave-induced and hardly influenced by aerodynamic load regardless of wind speed. It is thus proved that aerodynamic load has a limited influence on the wave frequency motions. Besides, strong response can be observed around the resonant frequency for both surge and pitch motions. Although aerodynamic load plays a tiny role on the wave frequency response, it nevertheless has a significant damping effect on the resonant response. Comparisons between case LC1, LC2 and LC3 manifest that wind force reduces the platform motions and such aerodynamic damping effect is mostly effective around the resonant frequency range.

301 *4.2 Nacelle acceleration*

302 Mechanical facilities installed inside the nacelle will bear inertial loads caused by nacelle
 303 accelerations. In the model test, nacelle accelerations along three directions are measured and
 304 statistical results of the recorded data are summarized in Table 9-11.

305 **Table 9**
 306 Statistical results of nacelle acceleration along X direction

Case No.	Max (m/s ²)	Min (m/s ²)	Mean (m/s ²)	Std. dev. (m/s ²)
LC1	1.752	-1.760	0.047	0.389
LC2	2.360	-1.222	0.583	0.451
LC3	2.573	-1.020	0.785	0.476

307 **Table 10**
 308 Statistical results of nacelle acceleration along Y direction

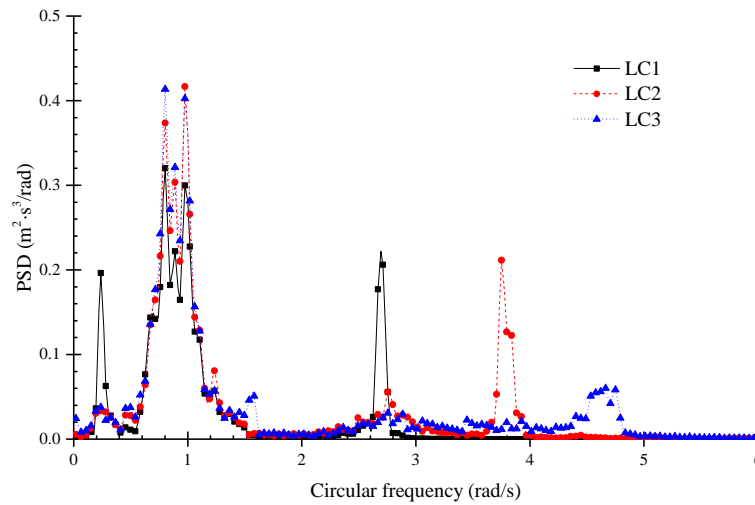
Case No.	Max (m/s ²)	Min (m/s ²)	Mean (m/s ²)	Std. dev. (m/s ²)
LC1	0.22	-0.123	0.05	0.047
LC2	1.239	-1.092	0.063	0.25
LC3	1.544	-1.495	0.073	0.38

309 **Table 11**
 310 Statistical results of nacelle acceleration along Z direction

Case No.	Max (m/s ²)	Min (m/s ²)	Mean (m/s ²)	Std. dev. (m/s ²)
LC1	0.489	-0.396	0.021	0.121
LC2	1.086	-1.044	0.027	0.223
LC3	1.077	-1.386	0.042	0.27

311
 312 Although the resonant motions of surge and pitch are reduced in the presence of wind
 313 force, the nacelle accelerations seem to be amplified by the wind force. As summarized in
 314 Table 9, the maximal value, the mean value and the standard deviation of nacelle acceleration
 315 are all somewhat augmented with the increase of wind speed. Acceleration in Y direction is
 316 also observed. As shown in Table 10, the standard deviation in case LC3 is about 8 times
 317 larger than that in case LC1. Such significant augment of standard deviation inherently
 318 implies the excitation of platform sway motion, which will be discussed in more detail in the
 319 following part of this paper. Although the wind mainly induces horizontal load, acceleration
 320 along vertical direction is still increased in Table 11 due to the coupling between pitch and
 321 heave. The statistical results indicate that large wind load is likely to cause significant nacelle
 322 acceleration. In order to present the characteristics of the accelerations more clearly, the

323 power spectrum density (PSD) of nacelle accelerations along X direction in the three test
324 cases are shown in Fig. 13.



325

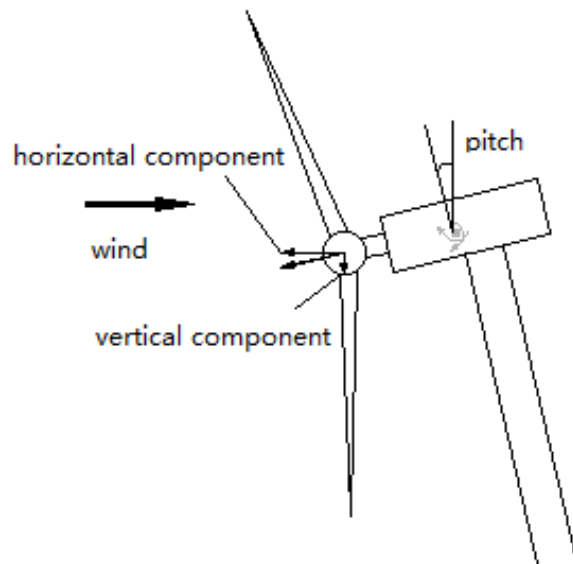
326 **Fig. 13.** Power spectrum density of nacelle acceleration along X direction.

327 In parked condition (LC1), it is wave force and tower structural vibration that dominate
328 the nacelle acceleration. According to LC1 curve, the nacelle acceleration is mainly excited
329 by linear wave force and a majority of response energy concentrates on the wave energy
330 frequency range. Another response peak is observed around 0.27 rad/s, which is close to pitch
331 resonant frequency. Apart from hydrodynamic excitations, the vibration of tower also
332 stimulates the nacelle acceleration. LC1 curve shows a substantial response peak at 2.68 rad/s,
333 which is close to the tower vibration frequency obtained by hammer test.

334 When the wind force is considered, a couple of extra frequency components appear in
335 the response. In addition to the response induced by wave force and tower vibration, the
336 nacelle acceleration is significantly excited around 3P rotor rotation frequency. As discussed
337 above, the rotor is purely driven by wind and the rotor speed keeps varying due to platform
338 motions. Therefore, the 3P rotation frequency in Fig. 13 is somewhat different from that in
339 Table 1. For LC2 and LC3 PSD curves, it can be seen that response amplitudes around pitch
340 resonant frequency and tower vibration frequency are substantially reduced. It inherently
341 manifests that pitch motion and tower vibration are suppressed. On the contrary, the nacelle
342 acceleration is amplified around wave energy frequency range with the consideration of wind
343 force.

344 *4.3 Effects of rotor rotation on yaw and roll motions*

345 Simulation cases LC4 and LC5 are selected to clarify the rotor rotation effect on
 346 platform motions. The wind turbine is parked in LC4 whereas the wind drives the rotor to
 347 rotate in LC5. As shown in Fig. 14 , the floating system is subject to an extra torque which is
 348 induced by the rotor. Due to pitch motion, the rotor torque is separated into a vertical
 349 component and a horizontal component. The vertical component induces gyroscopic loading
 350 and excites yaw motion while the horizontal component will lead to roll motion. Apparently,
 351 the two components vary with time and are governed by both incident wave frequency and
 352 pitch natural frequency of the floating system.



353
 354 **Fig. 14.** Horizontal and vertical components of rotor torque.

355 **Table 12**

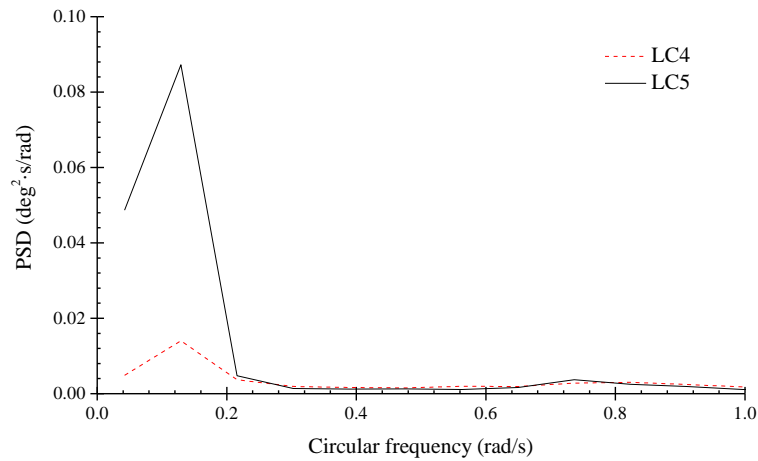
356 Statistical results of yaw motion

Case No.	Max (deg)	Min (deg)	Mean (deg)	Std. dev (deg)
LC4	0.321	-0.189	0.089	0.071
LC5	0.561	-0.311	0.157	0.127

357

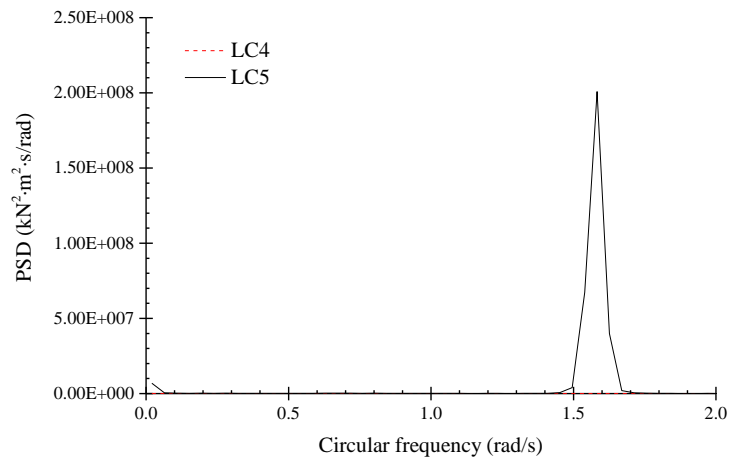
358 As listed in Table 12, the standard deviation of yaw motion in LC5 is nearly doubled
 359 compared with that in LC4. Besides, the mean position of yaw motion is kept at 0.157 deg
 360 with gyroscopic loading in LC5. It is caused by the non-zero average vertical torque
 361 components associated with inclined mean position of the platform. Rotor rotation effect is

362 mostly effective on the resonant response of yaw motion (see Fig. 15). Due to the symmetry
 363 geometry of the platform, yaw motion is seldom observed in LC4. Comparatively, yaw
 364 motion is excited significantly at about 0.14 rad/s by the gyroscopic loading, which is close to
 365 yaw natural frequency. Apart from inducing yaw motion, gyroscopic loading causes some
 366 unfavorable yaw bearing at the connection of the nacelle and the tower. The power spectrum
 367 density of yaw bearing at this connection position is displayed in Fig. 16. Although yaw
 368 motion is excited at its resonant frequency, it is interesting to find that the peak response of
 369 the yaw bearing is at 1.58 rad/s, which is close to the rotor rotation speed. It manifests that the
 370 yaw bearing is mainly induced by wind force.



371
 372

Fig. 15. Power spectrum density of yaw motion.

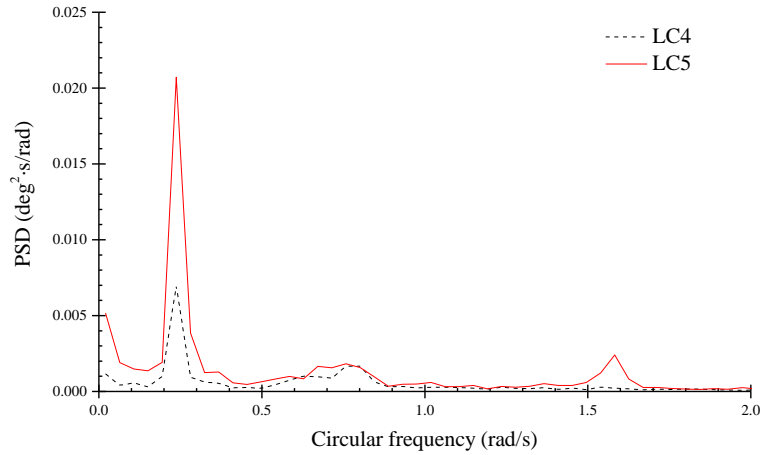


373
 374

Fig. 16. Power spectrum density of tower-top axial torque.

375 Similar to the gyroscopic loading, the horizontal component of the rotor torque will
 376 induce unfavorable roll motion as well. What's more, the resonant roll motion may be excited
 377 since the varying frequency of the horizontal component is very close to roll resonant
 378 frequency. Fig. 17 displays the power spectrum density curves of platform roll motion. It is

379 shown that the resonant roll motion is excited by the horizontal the rotor torque. Besides,
 380 low-frequency roll motion is observed due to the coupling between roll and sway motions.



381
 382

Fig. 17. Power spectrum density of roll motion

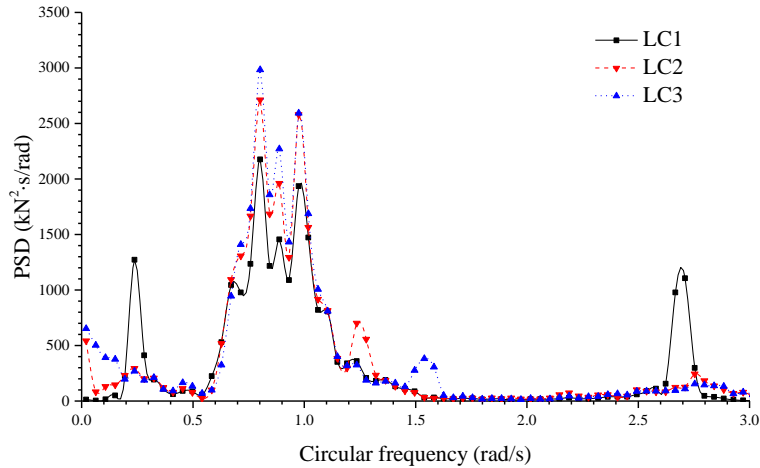
383 *4.4 Shaft axial force*

384 The measured shaft axial force consists of two components, namely the wind force
 385 applied on the rotor plane and the inertial force induced by the nacelle motions. Statistical
 386 results of the shaft axial force are summarized in Table 13. Alongside with the increase of
 387 wind force, the maximum, the minimum and the mean values of shaft axial force are all
 388 increased where just a little bit augment of the standard deviation is observed. It seems that
 389 the shaft axial force is mainly dominated by the inertial motions of the nacelle and wind force
 390 can be simplified as a constant linear superposition.

391 **Table 13**

392 Statistical results of shaft axial force for LC1, LC2 and LC3

Case No.	Max (kN)	Min (kN)	Mean (kN)	Std. dev (kN)
LC1	377.202	-478.436	41.699	98.686
LC2	1068.2	166.6	651.7	107.506
LC3	1334.76	506.562	909.342	117.6



393

394

Fig. 18. Power spectrum density of shaft axial force

395

Fig. 18 displays the frequency components of shaft axial force in the three test cases.

396

When the wind force is not considered, response peak can be found at pitch resonant

397

frequency, wave frequency and vibration frequency of the tower. Once the floating wind

398

turbine is subject to wind force, the response amplitudes at pitch resonant frequency and

399

tower vibration frequency are significantly reduced. Nevertheless, response within the wave

400

energy frequency range is somewhat amplified. It is easy to find that the response

401

characteristics of the shaft axial force and the nacelle acceleration are very similar (see Fig.

402

13), manifesting that the shaft axial force is mainly induced by nacelle inertial motions.

403

4.5 Tower-top shear force and bending moment

404

Tower top is a crucial connection point of the wind turbine, in terms of limited strength

405

and fatigue loads. As a changing point in the shape of the structure geometry, tower top is a

406

key point for fatigue strength check as well. Therefore, the extreme values and the varying

407

range of the shear force applied at the tower top are critical items in the dynamic response of

408

a floating wind turbine. Statistical data of the measured shear force are listed in Table 14.

409

410

411

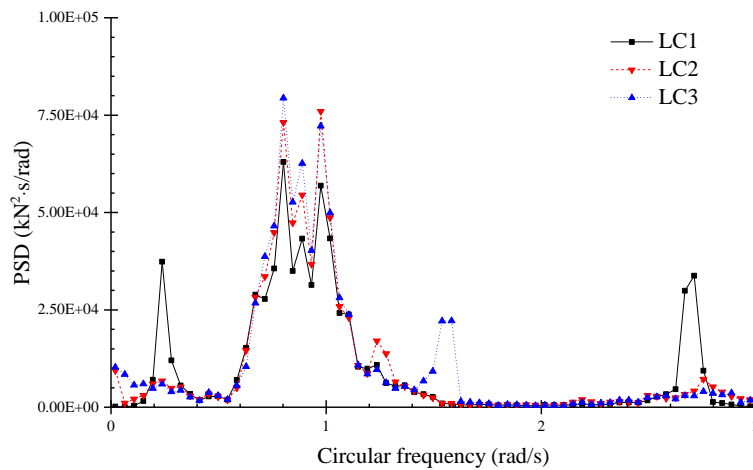
412 **Table 14**

413 Statistical results of shear force and bending moment

Term	Loading Case	Max	Min	Mean	Std. Dev
Shear force (kN)	LC1	753	-771	11	170
	LC2	1426	-39	796	176
	LC3	1709	316	1092	190
Bending moment (kN·m)	LC1	5003	-4485	129	1001
	LC2	2916	-12201	-4423	2812
	LC3	6117	-16503	-5957	3752

414

415 The PSD of the shear force is shown in Fig. 19, where multi-frequency components can
 416 be identified. In parked condition, shear force response is mainly dominated by three
 417 frequency components, namely the pitch resonant frequency, the wave energy frequency and
 418 the tower vibration frequency. It implies that shear force is both dominated by platform
 419 motions and tower structural dynamics. Once the wind force is considered, the shear force is
 420 diminished to a very low level at pitch resonant frequency and tower vibration frequency.
 421 Comparatively, the shear force exhibits increased response around wave energy frequency
 422 range.

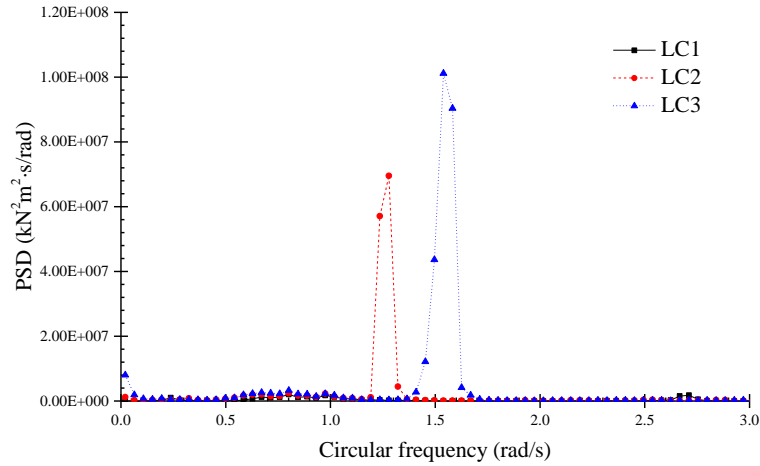


423

424

Fig. 19. Power spectrum density curves of tower-top shear force.

425



426
427 **Fig. 20.** Power spectrum density curves of tower-top bending moment.

428 Compared with the PSD curves of shear force, the PSD curves of bending moment are
429 mainly governed by aerodynamic loads in Fig. 20 while hydrodynamic excitation and tower
430 structural dynamics appear to have limited influence on the responses. As expected, the
431 responses are limited in parked condition. When the wind force is considered, the bending
432 moment is substantially excited at around 1P rotor rotation frequency (1.17 rad/s for LC2 and
433 1.5 rad/s for LC3) and the responses over other frequencies are nearly invisible.

434 *4.6 Dynamic characteristics of mooring system*

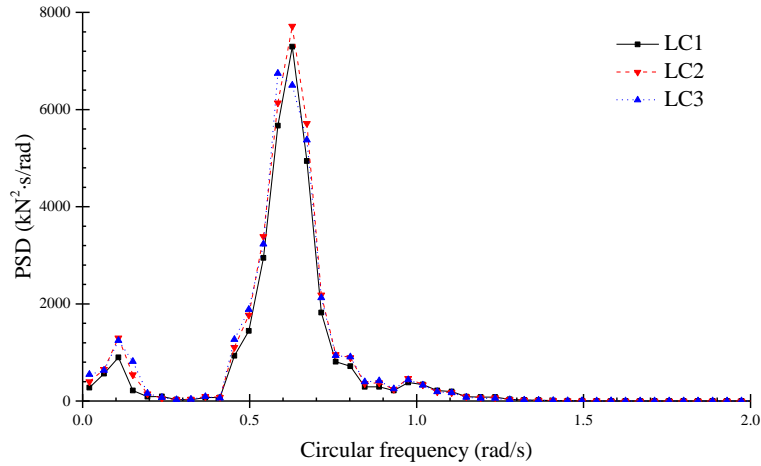
435 A floating wind turbine depends on the mooring system to maintain its position within an
436 acceptable range. Thus, the mooring system will bear the loads induced by platform motions.
437 The fairlead tension force of a selected mooring line is investigated in this section. Among the
438 three mooring lines, the line along 180 degree direction sustains the largest load (see Fig. 5)
439 and is therefore selected here. The statistical results of the mooring line tension are
440 summarized in Table 15, and the corresponding PSD curves are shown in Fig. 21.

441 **Table 15**

442 Statistical results of mooring line tension force (line 1)

Case No.	Max (kN)	Min (kN)	Mean (kN)	Std. dev (kN)
LC1	3981.74	1219.12	2576.42	350.94
LC2	4560.92	1673.84	3013.50	375.63
LC3	4752.02	1822.80	3188.92	375.73

443



444

445

Fig. 21. Power spectrum density of mooring line tension force (line 1).

446

447

448

449

450

451

452

453

454

455

456

457

458

459

460

From the data in Table 15 and the curves in Fig. 21, it indicates that the tension force is mainly induced by wave force while wind force can be simplified as a linear suppression. According to the statistical data, the maximum mooring line tension increases with the thrust force. Nevertheless, the standard deviation remains relatively stable regardless of wind speed. The PSD curves demonstrate that mooring line tension is mainly wave-induced and a majority of response concentrates within wave energy frequency and resonant frequency range. Besides, little discrepancy is observed between the three curves, indicating that wind force effect is limited. It is thus reasonable to simplify aerodynamic load as an extra constant superposition when analyze mooring line dynamics. Although mooring line tension is strongly dependent on platform motions, it is interesting to find that mooring tension exhibits instinctive response characters with aerodynamic loads compared to platform motions. It inherently indicates that a static or quasi-static method (stiffness matrix model & catenary line theory) is not applicable to capture the behavior of mooring system in a numerical modeling of floating wind turbine, as both categories of methods are exactly depended on platform motions.

461

5. Conclusions

462

463

464

This paper mainly addresses the model test research of a semisubmersible floating wind turbine. A new approach is proposed in this paper to correct the deficient thrust force problem in a Froude scale experimental condition. This approach uses the wind to drive the rotor rather

465 than using a motor. Compared with common correction ways, this approach can better
466 simulate the operation state of the rotor and the measured shaft axial torque is more realistic.
467 TSR can also be maintained to some extent which ensures that system excitation frequencies
468 resulting from rotor imbalance or aerodynamic interaction with the tower will possess the
469 correct frequency. Besides, it also overcomes some negative effects produced by common
470 correction ways. Conclusions drawn from the study in this paper are listed in the following.

471 1) Platform motions suffer damping effects from the wind force and this influence is mostly
472 effective around resonant frequency range. Although platform motions are reduced
473 considering aerodynamic effects, nacelle accelerations are nevertheless amplified a lot at
474 particular frequency zones by the wind force. Multi-frequency excitations are found in
475 the response, which is dominated by the tower dynamics and the wind force.

476 2) The motions of a floating wind turbines exhibit distinctive features due to rotor rotation.
477 It is observed that gyroscopic loading stimulates yaw motion even in head waves.
478 Meanwhile, the roll resonant motion is excited by the time-varying rotor torque.

479 3) Tower vibration is an important item for tower-top dynamic response. In the responses of
480 nacelle acceleration and shaft axial force, excitations have been observed around tower
481 vibration frequency. Nevertheless, no evidence is available showing that tower dynamics
482 has any influence on platform motion. It is also found that wind force can suppress tower
483 vibration.

484 4) Shear force applied at tower top is found to be governed by multi-frequency excitation
485 components. Shear force is excited at wave energy frequency, tower vibration frequency
486 and rotor rotation frequency, representing hydro-aero-elastic couplings. By suppressing
487 surge motion and tower vibration, wind force is able to reduce shear force around
488 particular frequency range.

489 5) In spite of the aerodynamic effects on platform motions and tower, a selected mooring
490 line appears to be governed by hydrodynamic loads alone and the wind force can be
491 simplified as an extra constant force.

492 **Acknowledgement**

493 The authors would like to acknowledge SKLOE (State Key Lab of Ocean Engineering)
494 in Shanghai Jiao Tong University for the model test research support. This work is also
495 supported by China Scholarship Council (No. 201506230127).

496 **References**

- 497 [1] F.G. Nielsen, T.D. Hanson, B. Skaare, Integrated dynamic analysis of floating offshore
498 wind turbines, 25th International Conference on Offshore Mechanics and Arctic Engineering,
499 American Society of Mechanical Engineers, 2006, pp. 671-679.
- 500 [2] D. Roddier, C. Cermelli, A. Aubault, A. Weinstein, WindFloat: A floating foundation for
501 offshore wind turbines, *Journal of Renewable and Sustainable Energy* 2(3) (2010) 033104.
- 502 [3] D. Roddier, C. Cermelli, A. Weinstein, WindFloat: A Floating Foundation for Offshore
503 Wind Turbines—Part I: Design Basis and Qualification Process, ASME 2009 28th
504 International Conference on Ocean, Offshore and Arctic Engineering, American Society of
505 Mechanical Engineers, 2009, pp. 845-853.
- 506 [4] C. Cermelli, D. Roddier, A. Aubault, WindFloat: A floating foundation for offshore wind
507 turbines—Part II: hydrodynamics analysis, ASME 2009 28th International Conference on
508 Ocean, Offshore and Arctic Engineering, American Society of Mechanical Engineers, 2009,
509 pp. 135-143.
- 510 [5] A. Aubault, C. Cermelli, D. Roddier, WindFloat: A Floating Foundation for Offshore Wind
511 Turbines—Part III: Structural Analysis, ASME 2009 28th International Conference on Ocean,
512 Offshore and Arctic Engineering, American Society of Mechanical Engineers, 2009, pp.
513 213-220.
- 514 [6] M. Karimirad, C. Michailides, V-shaped semisubmersible offshore wind turbine: An
515 alternative concept for offshore wind technology, *Renewable Energy* 83 (2015) 126-143.
- 516 [7] L. Li, Y. Gao, Z.M. Yuan, S. Day, Z.Q. Hu, Dynamic response and power production of an
517 integrated wind, wave and tidal energy system, *Renewable Energy* 116 (2017) 412-422.
- 518 [8] M. Borg, M. Collu, Offshore floating vertical axis wind turbines, dynamics modelling
519 state of the art. Part III: Hydrodynamics and coupled modelling approaches, *Renewable and*
520 *Sustainable Energy Reviews* 46 (2015) 296-310.
- 521 [9] H.R. Martin, Development of a scale model wind turbine for testing of offshore floating
522 wind turbine systems, University of Maine, 2011.
- 523 [10] R. Farrugia, T. Sant, D. Micallef, A study on the aerodynamics of a floating wind turbine
524 rotor, *Renewable Energy* 86 (2016) 770-784.
- 525 [11] S. Salehyar, Q. Zhu, Aerodynamic dissipation effects on the rotating blades of floating
526 wind turbines, *Renewable Energy* 78 (2015) 119-127.
- 527 [12] T.J. Larsen, T.D. Hanson, A method to avoid negative damped low frequent tower
528 vibrations for a floating, pitch controlled wind turbine, *Journal of Physics: Conference Series*,
529 IOP Publishing, 2007, p. 012073.

530 [13] P.F. Odgaard, L.F. Larsen, R. Wisniewski, T.G. Hovgaard, On using pareto optimality to
531 tune a linear model predictive controller for wind turbines, *Renewable Energy* 87 (2016)
532 884-891.

533 [14] J.M. Jonkman, Dynamics modeling and loads analysis of an offshore floating wind
534 turbine, University of Colorado, 2007.

535 [15] B. Skaare, T.D. Hanson, F.G. Nielsen, R. Yttervik, A.M. Hansen, K. Thomsen, T.J.
536 Larsen, Integrated dynamic analysis of floating offshore wind turbines, *European Wind*
537 *Energy Conference*, Milan, Italy, 2007, pp. 7-10.

538 [16] L. Li, Z.Q. Hu, J. Wang, Y. Ma, Development and Validation of an Aero-hydro
539 Simulation Code for Offshore Floating Wind Turbine, *J Ocean Wind Energy* 2(1) (2015) 1-11.

540 [17] S. Quallen, T. Xing, CFD simulation of a floating offshore wind turbine system using a
541 variable-speed generator-torque controller, *Renewable Energy* 97 (2016) 230-242.

542 [18] P. Passon, M. Kühn, S. Butterfield, J. Jonkman, T. Camp, T.J. Larsen, OC3—benchmark
543 exercise of aero-elastic offshore wind turbine codes, *Journal of Physics: Conference Series*,
544 IOP Publishing, 2007, p. 012071.

545 [19] F. Vorpahl, W. Popko, IEA Wind Annex 30—OC4 project. The offshore code comparison
546 collaboration continuation, IEA wind side event at EWEA 2011 annual event, Brussels,
547 Belgium, 2011.

548 [20] F. Duan, Z.Q. Hu, J.M. Niedzwecki, Model test investigation of a spar floating wind
549 turbine, *Marine Structures* 49 (2016) 76-96.

550 [21] A.J. Coulling, A.J. Goupee, A.N. Robertson, J.M. Jonkman, H.J. Dagher, Validation of a
551 FAST semi-submersible floating wind turbine numerical model with DeepCwind test data,
552 *Journal of Renewable and Sustainable Energy* 5(2) (2013) 023116.

553 [22] M. Drela, XFOIL: An analysis and design system for low Reynolds number airfoils, *Low*
554 *Reynolds number aerodynamics*, Springer1989, pp. 1-12.

555 [23] J.M. Jonkman, M.L. Buhl Jr, FAST User's Guide, National Renewable Energy
556 Laboratory (NREL), 2005.

557 [24] H.R. Martin, R.W. Kimball, A.M. Viselli, A.J. Goupee, Methodology for Wind/Wave
558 Basin Testing of Floating Offshore Wind Turbines, *Journal of Offshore Mechanics and Arctic*
559 *Engineering* 136(2) (2014) 020905.

560 [25] J.M. Jonkman, S. Butterfield, W. Musial, G. Scott, Definition of a 5-MW reference wind
561 turbine for offshore system development, National Renewable Energy Laboratory Golden,
562 CO, 2009.

563 [26] F. Duan, Z. Hu, J. Wang, Model Tests of a Spar-Type Floating Wind Turbine Under
564 Wind/Wave Loads, ASME 2015 34th International Conference on Ocean, Offshore and Arctic
565 Engineering, American Society of Mechanical Engineers, 2015.

566